PNAS RESEARCH ARTICLE | PHYSICS OPEN ACCESS

Observation of the most H_2-dense filled ice under high pressure

Umbertoluca Ranieri[a,b,1], Simone Di Cataldo[a,c,1], Maria Rescigno[a,d], Lorenzo Monacelli[e], Richard Gaal[d], Mario Santoro[f,g], Leon Andriambariarijaona[h], Paraskevas Parisiades[h], Cristiano De Michele[a], and Livia Eleonora Bove[a,d,h,2]

Edited by Pablo Debenedetti, Princeton University, Princeton, NJ; received July 26, 2023; accepted October 30, 2023

Hydrogen hydrates are among the basic constituents of our solar system's outer planets, some of their moons, as well Neptune-like exo-planets. The details of their high-pressure phases and their thermodynamic conditions of formation and stability are fundamental information for establishing the presence of hydrogen hydrates in the interior of those celestial bodies, for example, against the presence of the pure components (water ice and molecular hydrogen). Here, we report a synthesis path and experimental observation, by X-ray diffraction and Raman spectroscopy measurements, of the most H_2-dense phase of hydrogen hydrate so far reported, namely the compound 3 (or C_3). The detailed characterisation of this hydrogen-filled ice, based on the crystal structure of cubic ice I (ice I*c*), is performed by comparing the experimental observations with first-principles calculations based on density functional theory and the stochastic self-consistent harmonic approximation. We observe that the extreme (up to 90 GPa and likely beyond) pressure stability of this hydrate phase is due to the close-packed geometry of the hydrogen molecules caged in the ice I*c* skeleton.

clathrate hydrates | phase transitions | high pressure | Raman | ab initio simulations

Significance

Clathrate hydrates of methane and other alkanes are a natural part of the deep-sea and permafrost environments and important gas reservoirs. Still other gas hydrate phases, not (yet) known in nature, have been characterized in the laboratory. Here, combination of high pressures and high temperatures was used to synthesize a hydrogen hydrate phase which has the structure of cubic ice for the water framework and twice as many H_2 as H_2O molecules in the unit cell, namely the highest gas-to-water molar ratio reported to date in any crystalline solid made of water and gas. This water–hydrogen compound is most likely stable up to pressures beyond the limit of the current experiments and might be abundant inside extra-terrestrial objects.

Gas hydrates are probably more abundant than rocky materials or all polymorphs of pure ice in giant icy and gaseous planets like Jupiter, Saturn, Uranus, and Neptune, as well as in Neptune-like exo-planets, and hydrogen hydrate must account for a significant part of them. These planets have a H_2 and He gases–dominated atmosphere and an interior mostly constituted by planetary ices (H_2O, CH_4, and NH_3) subjected to high pressure and temperature. Molecular hydrogen potentially contributes significantly to the volatile budget of other water-rich objects of various sizes, as witnessed by the detection of H_2 in the vapour plume of Saturn's tiny moon Enceladus, in abundances comparable to NH_3 and CO_2 (1) or in other trans-Neptunian objects (2, 3). The presence of H_2 in significant amount may have a major impact on the planetary habitability, by affecting both atmospheric thermal budget and interior redox state, particularly in water-rich worlds (4). Depending on the size of the planet or moon, H_2 may be incorporated in the planetary interior in different (solid) hydrate phases binding the gas at fairly high temperatures. The crystalline structure formed and the fraction of hydrogen stored in these systems depend on the specific thermodynamic conditions.

Laboratory experiments have indeed discovered that mixtures of water (or ice) and hydrogen gas spontaneously crystallize into a hydrogen clathrate hydrate under moderate pressures (above 0.1 GPa at temperatures below 270 K) (5). This non-stoichiometric guest–host compound is characterized by polyhedral cavities constituted of hydrogen-bonded water molecules encaging a variable amount of H_2 molecules in the well-known clathrate structure II (or sII), which is also observed for the hydrates of other gas species (6). Such a phase provides a higher stability for H_2 when compared to its pure phase sublimation equilibrium. As for some other gas hydrates, at higher pressures, the so-called "filled ice" structures form, in which the water host sublattice is no longer formed by cages but resembles one of the crystalline phases of pure water ice (7, 8). Upon compression, hydrogen hydrate goes through a sequence of phase transitions into a variety of crystalline phases with generally an increasing fraction of H_2 molecules per H_2O. In addition to sII, the phases C_{-1} (9), C_0 (10–12), C_1 (13), C_1' (14), and C_2 (13) have been reported over the pressure range up to ~3 GPa. Yet, this variety is small compared to the structural diversity exhibited by the many water ice phases (15, 16), and it is likely that new hydrogen hydrate compounds remain to be discovered. In phase C_2, the water sublattice forms the cubic ice I*c* structure and the H_2 to H_2O molar ratio is of 1. Another phase, called C_3, which should share its water sublattice with C_2 and should have an extremely high H_2 to H_2O molar ratio of 2, was calculated to become stable above 38 GPa (17) but no experimental observation of this new hydrate exists so far. While several computational (18–22) studies of hydrogen hydrates at high pressure have been previously reported, the only experimental datasets existing above 3 GPa in the literature essentially come

Author contributions: L.E.B. designed research; U.R., S.D.C., M.R., L.M., R.G., M.S., L.A., P.P., and L.E.B. performed research; U.R., S.D.C., M.R., C.D.M., and L.E.B. analyzed data; and U.R., S.D.C., and L.E.B. wrote the paper.

The authors declare no competing interest.

This article is a PNAS Direct Submission.

[1]U.R. and S.D.C. contributed equally to this work.

[2]To whom correspondence may be addressed. Email: livia.bove@epfl.ch.

This article contains supporting information online at https://www.pnas.org/lookup/suppl/doi:10.1073/pnas.2312665120/-/DCSupplemental.

Published December 18, 2023.

from a single group (23–25). The authors showed the stability of hydrogen hydrate upon compression to 70 GPa by Raman spectroscopy and reported the observation of a small tetragonal distortion of the high-pressure C_2 phase above 20 GPa by X-ray diffraction (XRD), followed by a structural transition to an unsolved phase at about 45 GPa (which is not the predicted C_3 phase) (24). Another study reported no structural transition at 45 GPa but pressure-induced amorphization at 65 GPa for the D_2O–H_2 system (not for H_2O–H_2) (25).

The existence of the elusive C_3 phase thus remains to be proven, and the consequences of it on the volatile balance of large icy and gas planets' atmospheres and on the modelling of their interior to be investigated. Furthermore, the C_3 phase would be the most gas-rich hydrate ever discovered, with a hydrogen volume density higher than 0.25 kg/L, i.e., four times that of liquid H_2, stored in a non-reactive, environmentally favorable water frame. Unveiling the conditions of formation of this remarkable hydrogen-dense hydrate, understanding the way water and hydrogen can fit in such a tight volume minimizing their repulsive interaction, and probing the possibility to recover such a structure at ambient pressure would pave the way to new opportunities of storage of hydrogen at high concentrations in hydrates. Hydrates constitute indeed a technologically attractive hosting environment for physical H_2 storage due to their appealing properties such as low energy consumption for charge and discharge, safety, cost-effectiveness, and environmentally friendly nature (26). The identification of a hydrogen hydrate phase trapping hydrogen at mass fractions surpassing those of the best materials presently used for hydrogen storage would boost the research for devising ways to increase H_2 storage capacity at more realistic engineering pressures.

In this work, we investigate the room-temperature and high-pressure binary phase diagram of water and hydrogen by coupling synchrotron XRD and Raman spectroscopy measurements in a diamond anvil cell (DAC) up to 90 GPa. In some experimental runs, laser heating (LH) of the sample was employed at 40 GPa to overcome possible kinetic barriers preventing the transition to the thermodynamic ground state. First-principles calculations based on evolutionary algorithms for crystal structure prediction (27, 28), density functional theory (DFT), and the stochastic self-consistent harmonic approximation (SSCHA) (29, 30) were employed to accurately simulate the structural, thermodynamical, dynamical, and optical properties of the studied phases. Our results demonstrate the existence of the predicted (17) hydrogen-dense C_3 phase, giving a rationale for its synthesis, as well as an explanation of the lack of its observation in previous experiments. The paper is structured as follows: First, we will present the computational and experimental results (from XRD and then Raman spectroscopy), and then, we will discuss the peculiar structural features of the C_3 phase that enable its stability up to Megabar pressures.

Results

We computed the phase diagram of hydrogen and water using ab initio crystal structure prediction based on density functional theory at 20, 40, and 200 GPa and computed the equation of state of stable phases at a large number of intermediate pressures (see *SI Appendix* for further details and *SI Appendix*, Figs. S1–S6 therein). Fig. 1 shows a summary of the pressure stability of the different hydrogen hydrate phases. Computationally, we find the C_2 phase to be stable up to about 20 GPa, while the C_3 phase becomes stable only above 30 GPa (see the calculated enthalpy in *SI Appendix*, Fig. S4) leaving a region of about 10 GPa in which no hydrate phase is stable. However, as we will discuss more in-depth below, the C_2 phase can experimentally remain metastable up to higher pressures, and only when sufficiently heated, it transforms into the C_3 phase, which is then observed up to the highest investigated pressure of this work (90 GPa). On the other hand, the samples that were compressed without laser heating remained in the C_2 phase, which is metastable up to the highest investigated pressure (Fig. 1).

More than ten different Raman experiments have been performed on as many sample loadings and three of them have been coupled to synchrotron XRD measurements. In three of the experimental runs, laser heating was employed, heating the sample to 1,200(200) K at about 40 GPa, followed by rapid cooling (quenching) due to the high thermal conductivity of diamond. The high-pressure cells had been loaded at liquid nitrogen temperature with hydrogen hydrate samples in the clathrate phase sII, which formed the C_2 phase and excess water ice (because of the difference in composition between the sII and C_2 hydrogen hydrates) upon compression to pressures above 2–3 GPa, as expected from the extensive previous literature. Upon further compression to about 20 GPa and above, we start observing progressive appearance of pure solid H_2 in the sample (clearly identified by its Raman vibron signal), highly likely because of partial decomposition of hydrogen hydrate into its components, which is consistent with the region of instability in Fig. 1. For further details on the sample preparation and experimental setups, as well as computational details, we refer the reader to see *Materials and Methods*.

XRD Measurements and Related Computational Results. In Fig. 2, we report examples of XRD 2D images and patterns,

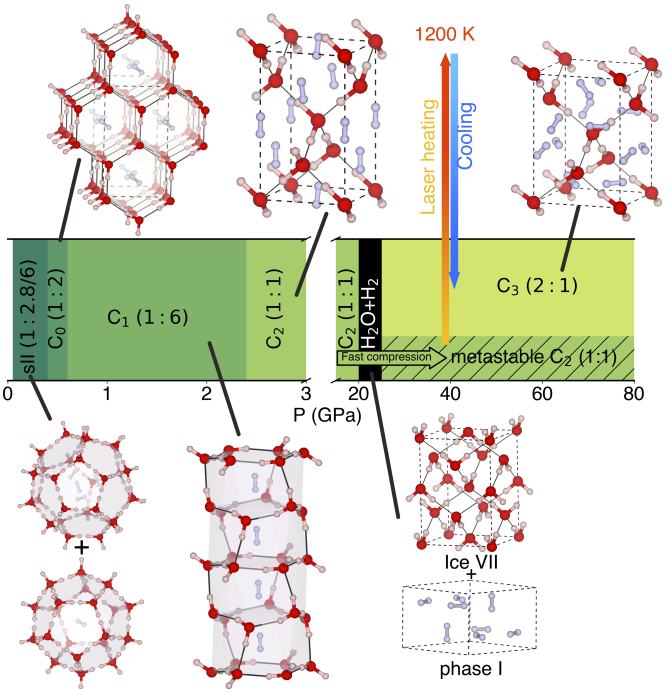

Fig. 1. Calculated structural transition sequence of hydrogen hydrate as a function of pressure, with regions of thermodynamical stability of different phases indicated by different colors. H_2:H_2O molar ratios are reported in parenthesis. "H_2O+H_2" indicates that no hydrate phase is thermodynamically stable in the corresponding pressure range. Ball-and-stick models of the crystal structures are also reported (O atoms in red, H atoms in white, and H_2 molecules in cyan). Experimentally, phase C_2 can be compressed to pressures above its range of stability as a metastable phase. Upon laser heating at about 40 GPa, it transforms into phase C_3.

before and after laser heating of the sample, as well as the obtained pressure–volume equations of state for the phases C_2 and C_3, which we also compare to the results of our numerical simulations. The C_2 and C_3 phases, which feature proton-disordered H_2O molecules and rotationally disordered H_2 molecules, can be described by the same cubic space group $Fd\bar{3}m$. With the origin choice 1, the O atoms sit in the 8*a* position (0, 0, 0) and the center of mass of the H_2 molecules sit in either the 8*b* position (1/2, 1/2, 1/2) for C_2 or the 16*d* position (5/8, 5/8, 5/8) for C_3. Although the patterns of the C_2 and C_3 phases can be explained by the same space group, the two are easily distinguished due to the markedly different volume. This striking expansion of the water framework is due to the massive uptaking of H_2 molecules which double in number in C_3 with respect to the C_2 phase.

In the measurements before LH of the sample, our results point to the presence of the C_2 phase, persisting in a metastable state at all pressures. The obtained volumes for C_2 are in good agreement with the previous studies (13, 24, 33). Conversely, upon LH at about 40 GPa, we observe a clear change in the XRD pattern (Fig. 2 *A* and *B*) that corresponds to a volume increase of about 20% for hydrogen hydrate (Fig. 2*C*). The measured diffraction patterns, the equation of state, and the volume change are all in excellent agreement with the computational results for a transition from the C_2 to the C_3 phase. When C_3 forms at 40 GPa, its cubic unit cell has a volume of about 200 $Å^3$ and contains 16 H_2 molecules. This corresponds to approx. 0.27 kg/L of H_2 (not including the hydrogen of the water). For reference, the H_2 weight % of the C_3 phase is 18.3. Once formed, C_3 remains stable up to the highest measured pressure.

Raman Spectroscopy Measurements and Related Computational Results. The results from the Raman measurements are summarized in Fig. 3, where we show selected spectra for the C_2 and C_3 phases as a function of pressure along different thermodynamic paths—with and without laser heating—along with their simulated spectra, as well as the H_2 vibron frequencies versus pressure. As we will discuss in the following, the measured Raman spectrum becomes substantially different depending on whether LH is applied or not.

In Fig. 3, *Left*, we report the measured Raman spectra and frequencies as a function of pressure in two different sets of experiments in which LH was not applied. The Raman spectrum of the C_2 phase is characterized by a single peak (the peak at about 4,250 cm^{-1} is due to the excess pure hydrogen in the sample), which becomes broader and whose frequency becomes higher as pressure increases. This peak is due to the vibron mode of the H_2 units in the structure. The observed extreme blueshift (mode hardening) with pressure is unlike in pure H_2, which exhibits a maximum frequency at approximately 38 GPa (34). The measured frequency for C_2, as well as its pressure dependence, is in excellent agreement with the previous literature (17, 23, 25, 33) and with our computed values. As shown in Fig. 3 *A*, *Left*, no other distinct peak appears, except for an extremely broad peak centered around 4,400 cm^{-1}, the frequency of which is substantially independent of pressure. This peak, which is hardly distinguishable from the background, probably stems from hydrogen being trapped in an amorphous form of hydrogen hydrate. In the samples on which we did not use LH, the C_2 phase persists up to the maximum investigated pressure of 90 GPa.

As shown in Fig. 3, *Right*, when LH is applied at 42 GPa, the Raman spectrum changes quite drastically: A total of three additional peaks appear at 4,480, 4,450, and 4,400 cm^{-1}. This observation is consistent with a transition from the C_2 to the C_3 phase, induced by the LH. The C_3 phase presents multiple peaks (see bottom spectrum of Fig. 3 *B*, *Right*) due to the presence of two symmetry-inequivalent H_2 molecules. In particular, while the centers of mass are equivalent, their lowest-energy orientations are not. Hence, on a qualitative level, the C_2 and C_3 phases can be distinguished by the occurrence of a series of satellite peaks in a range 200 cm^{-1} below the main

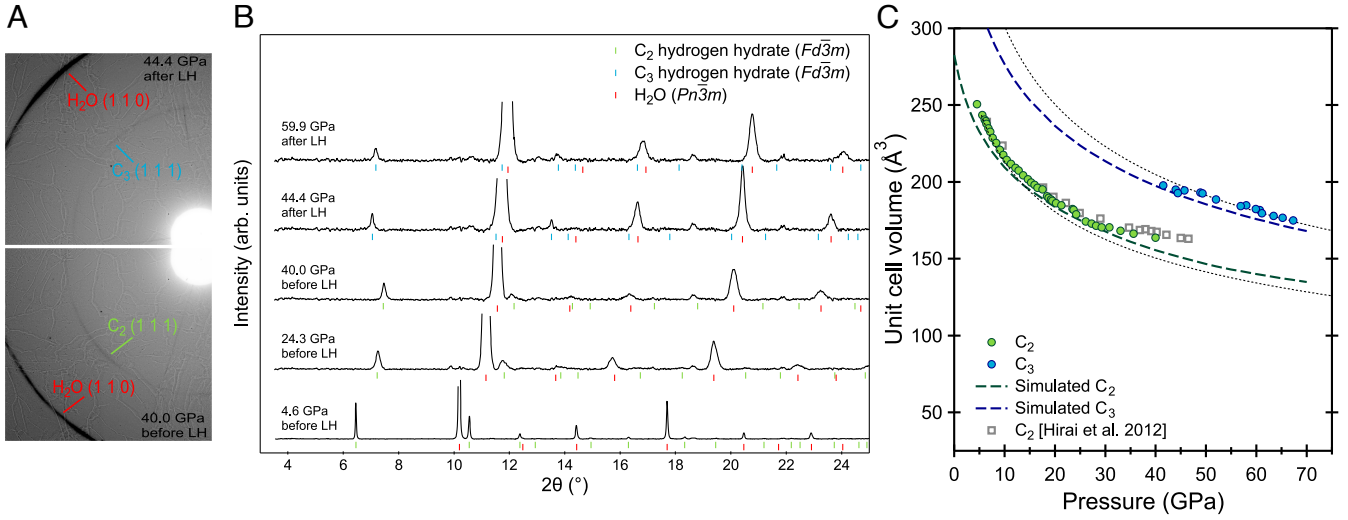

Fig. 2. XRD images (*A*) and patterns (*B*), and obtained volumes (*C*). (*A*) Details of two XRD images taken before and after laser heating, showing the first (and most intense) peak of hydrogen hydrate and of excess water ice. (*B*) Representative XRD patterns ($\lambda = 0.41$ Å) measured upon compression, before and after laser heating of the sample. The main (1 1 0) reflection of H_2O is not plotted entirely. The ticks correspond to the Bragg reflections of the refined structures: $(H_2O)H_2$ C_2 and $(H_2O)(H_2)_2$ C_3 hydrogen hydrate (both with space group $Fd\bar{3}m$), and H_2O ice VII (space group $Pn\bar{3}m$). The two weak peaks whose positions (18.65° and 21.9°) do not change with pressure are residual intensity from the masked diamond anvil peaks. (*C*) Unit cell volumes ($Z = 8$) as a function of pressure. Symbols represent experimental volumes and the values given in ref. 24 are reported as well. Dashed lines represent volumes derived from our DFT calculations and dotted lines represent the volumes of ideal mixtures of the equivalent amount of H_2O and H_2 molecules, calculated using the previously determined equations of state (31, 32).

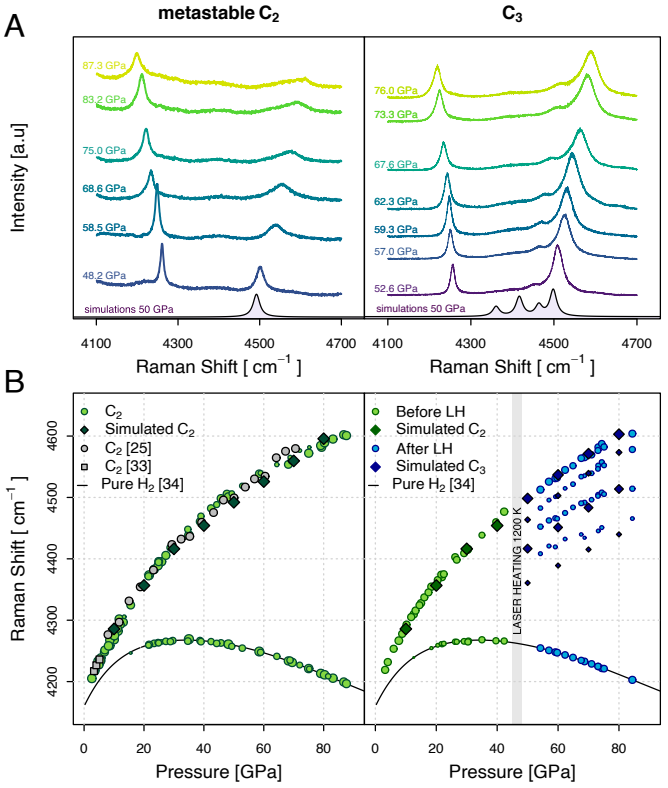

Fig. 3. Raman spectra (*A*) and vibron frequencies (*B*) for C_2 (*Left*) and C_3 (*Right*). (*A*) Representative experimental Raman spectra for the H_2 vibron at various pressures for the metastable C_2 (*Left*) and C_3 (*Right*) phases. Simulated Raman spectra at 50 GPa including an arbitrary frequency resolution are shown as black lines with filled areas for comparison. (*B*) Measured and calculated frequencies as a function of pressure for the C_2 (*Left*) and C_3 (*Right*) phase. The simulated frequencies account for both anharmonicity and DFT errors in the exchange-correlation functional as a uniform (pressure-independent) shift in frequency determined ab initio, whose details are reported in *SI Appendix*. The measured frequencies for the C_2 and C_3 phases are shown as green and blue dots, respectively. The calculated frequencies are shown as darker diamonds. Literature experimental data for the C_2 phase (25, 33) (gray symbols) and for pure solid H_2 (34) (black line) are also reported.

one. The computed phonon eigenvectors at the Γ point reveal how the differences in the environment of nonequivalent H_2 molecules (*SI Appendix*, Fig. S6) lead to substantially different energies in the H_2 vibron. The eight H_2 molecules in each primitive cell fall into two nonequivalent groups, based on their orientation with respect to the nearest oxygen atom. In particular, the observed peaks in order of increasing frequency correspond to the symmetric stretching of H_2 molecules pointing toward the nearest oxygen atom, the in- and out-of-phase stretching of all H_2 molecules, and the in- and out-of-phase stretching of H_2 molecules pointing orthogonally to the nearest oxygen atom, respectively. In simple terms, hydrogen atoms with their axis pointing toward the nearest oxygen atom exhibit a lower vibrational frequency than those pointing away from it, due to the induced perturbation from the excess negative charge around oxygen (*SI Appendix*, Fig. S6). Although these vibrational peaks become broader, they do remain visible up to the highest pressure measured.

Discussion

Summarizing the results of our XRD and Raman spectroscopy measurements, and the insight derived from our DFT and SSCHA calculations, we can finally reconcile all previous high-pressure experiments within a single picture. From about 20 GPa, the C_2 phase starts to decompose into its components; this is because in the pressure range between approx. 20 and 30 GPa, the separated phases of pure water and hydrogen are more stable than both C_2 and C_3, as shown by our calculated enthalpy (*SI Appendix*, Fig. S4). This explains the appearance of the pure H_2 Raman vibron peak from about 20 GPa, which is also present in previous data (23). If the region of decomposition is avoided through fast compression (compression rate of ∼5 GPa/s, as compared to a standard rate of typically 5 GPa/h), then no pure hydrogen is produced and we can follow the pressure shift of the C_2 Raman vibron peak without other contributions, as shown in *SI Appendix*, Fig. S7. As originally predicted in ref. 17, the C_3 phase is thermodynamically stable above approximately 30 GPa. However, at this pressure, the dense cubic ice framework prevents hydrogen diffusion, hence the C_2 phase can remain in a metastable state up to much higher pressures. This kinetic barrier can be overcome only by heating the sample and assuring hydrogen mobility, in the presence of a hydrogen basin. Indeed, we observe here that upon LH up to about 1,200 K, the system is able to overcome the barrier that separates it from the C_3 phase. Our computational results (*SI Appendix*, Figs. S8 and S9) also predict that upon compression of the C_2 phase above 20 GPa, the hydrogen molecules start to orient along the *c* axis, the hexagons of the water network elongate along the same direction, and the crystal symmetry is reduced from cubic to tetragonal, as observed in ref. 24. At even higher pressures, these local domains of symmetry-broken phases can favor amorphization due to the anisotropic compressibility of the C_2 phase, as observed in ref. 25. A similar guest orientational ordering was detected in the high-pressure phase III of methane hydrate (35, 36), before transition into a different structure at higher pressures.

We now discuss in further detail the structural properties of the high-pressure C_2 and C_3 phases. Despite sharing the same cubic ice skeleton for the water molecules, the C_2 and C_3 structures present a few key differences. These become clearer by considering the center of mass of the H_2 molecules (from here on named HCM), as shown in Fig. 4. In the C_2 phase, oxygens and HCMs form two identical diamond-like sublattices shifted by a $(1/2, 1/2, 0)$ vector (Fig. 4*C*). Indeed, at 40 GPa, the first O–O and H_2–H_2 distances are identical and equal to 2.35 Å (Fig. 4*A*). In the C_3 phase, however, the HCM network is markedly denser while the oxygen one expands; at the same pressure of 40 GPa, the nearest-neighbor H_2–H_2 distances are of about 2.0 Å , while the nearest neighbor O–O distances are of 2.5 Å (Fig. 4*B*): The oxygen sublattice has expanded to welcome further hydrogen molecules, which are thus closer packed. The HCMs form a network of corner-sharing tetrahedra (Fig. 4*D*) similar to those found in pyrochlores (37). Oxygen atoms sit at the center of a truncated tetrahedron (Fig. 4*E*), which consists of four hexagonal and four triangular faces. The vertexes of the truncated tetrahedron are occupied by HCMs, which implies that each oxygen is 12 coordinated with H_2 units. The hydrogen bond between water molecules, which ideally connects two oxygen atoms, passes through the center of one hexagon and is orthogonal to its plane (Fig. 4*E*). Intermolecular distances over a range of pressures up to 70 GPa are reported in *SI Appendix*, Fig. S9, where it is interesting to notice that the nearest-neighbor H_2-H_2 distances are very short in C_3 [shorter than in pure solid H_2 (32) at the same pressure].

To the best of our knowledge, the close-packed geometry of HCMs in the C_3 phase has never been observed in other filled